



**HAL**  
open science

## Tectonic nature and seismic response of top-basement detachment faults in magma-poor rifted margins.

A. Hölker,, Gianreto Manatschal, K Holliger,, D. Bernoulli

### ► To cite this version:

A. Hölker,, Gianreto Manatschal, K Holliger,, D. Bernoulli. Tectonic nature and seismic response of top-basement detachment faults in magma-poor rifted margins.. *Tectonics*, 2003, 22, pp.1035. 10.1029/2001TC001347 . hal-01253769

**HAL Id: hal-01253769**

**<https://hal.science/hal-01253769>**

Submitted on 28 Jan 2021

**HAL** is a multi-disciplinary open access archive for the deposit and dissemination of scientific research documents, whether they are published or not. The documents may come from teaching and research institutions in France or abroad, or from public or private research centers.

L'archive ouverte pluridisciplinaire **HAL**, est destinée au dépôt et à la diffusion de documents scientifiques de niveau recherche, publiés ou non, émanant des établissements d'enseignement et de recherche français ou étrangers, des laboratoires publics ou privés.

# Tectonic nature and seismic response of top-basement detachment faults in magma-poor rifted margins

Andreas B. Hölker<sup>1</sup>

Department of Earth Sciences, Swiss Federal Institute of Technology, Zurich, Switzerland

Gianreto Manatschal

CGS-EOST, CNRS - Université Louis Pasteur, Strasbourg, France

Klaus Holliger

Department of Earth Sciences, Swiss Federal Institute of Technology, Zurich, Switzerland

Daniel Bernoulli<sup>2</sup>

Department of Earth Sciences, Swiss Federal Institute of Technology, Zurich, Switzerland

Received 24 November 2001; revised 30 November 2002; accepted 6 March 2003; published 31 July 2003.

[1] Top-basement detachment faults (TBDF) represent exhumed segments of downward-concave detachments accommodating tens of kilometers of offset. TBDFs are key structures of magma-poor rifted margins, but are difficult to identify in seismic profiles, because they coincide with top-basement reflections. We have constructed realistic seismic models of an Alpine example, which were used to simulate full marine seismic surveys and to identify the seismic fingerprint of TBDFs in CMP-stacked and time-migrated sections. Minor extensional allochthons, which locally cap TBDFs, give rise to pronounced diffractions, which are in stark contrast to continuous reflections from uncapped segments of TBDFs. In time-migrated synthetic sections we find a continuous and constant amplitude reflection alternating with a laterally discontinuous reflection of variable amplitude. These diagnostics were also identified in the Lusigal 12 seismic profile imaging the Hobby High detachment, a TBDF in the Iberia Abyssal Plain. Using these diagnostics, small extensional allochthons and high-angle faults cutting the Hobby High detachment are observed in Lusigal 12 and the entire sedimentary cover can be shown to be postrift. *INDEX TERMS*: 8109 Tectonophysics: Continental tectonics—extensional (0905); 8105 Tectonophysics: Continental margins and sedimentary basins (1212); 3025 Marine Geology and Geophysics: Marine seismics (0935); 0935 Exploration Geophysics: Seismic methods (3025); *KEYWORDS*: rifted margins, top-basement detachment, faults,

extensional allochthons, downward concave detachment faults, seismic response, seismic modeling. **Citation**: Hölker, A. B., G. Manatschal, K. Holliger, and D. Bernoulli, Tectonic nature and seismic response of top-basement detachment faults in magma-poor rifted margins, *Tectonics*, 22(4), 1035, doi:10.1029/2001TC001347, 2003.

## 1. Introduction

[2] Top-basement detachment faults are parts of low-angle detachment systems. They represent the no longer active segments of downward-concave detachment faults which exhumed continental basement or mantle rocks at the seafloor. Their former hanging walls typically form extensional allochthons stranded along the trace of the fault. Examples of such faults have been extensively studied in the exposed ocean continent transition (OCT) zones of the ancient Tethyan margins in the Alps [Froitzheim and Eberli, 1990; Florineth and Froitzheim, 1994; Froitzheim and Manatschal, 1996; Manatschal and Nievergelt, 1997; Froitzheim and Rubatto, 1998]. Top-basement detachment faults have also been drilled in the west Iberian margin [Whitmarsh et al., 1998; Manatschal et al., 2001] as well as in the Woodlark basin (Papua New Guinea) [Taylor et al., 1999].

[3] The discovery of top-basement detachment faults has changed dramatically our views regarding the architecture and tectonic evolution of OCT zones in magma-poor margins. In particular, estimates of total strain (e.g.,  $\beta$ -factors) and hence also estimates of the strain rates are virtually impossible. Estimates of  $\beta$ -factors obtained from the interpretation of seismic data, may therefore have to be revised significantly, and a corresponding reinterpretation of seismic profiles across OCT zones could be indicated. An adequate determination of  $\beta$ -factors is of particular importance, because they form the basis of most isostasy and magma production models for rifted margins.

<sup>1</sup>Now at Proseis AG, Zurich, Switzerland.

<sup>2</sup>Now at Department of Earth Sciences, University of Basel, Switzerland.

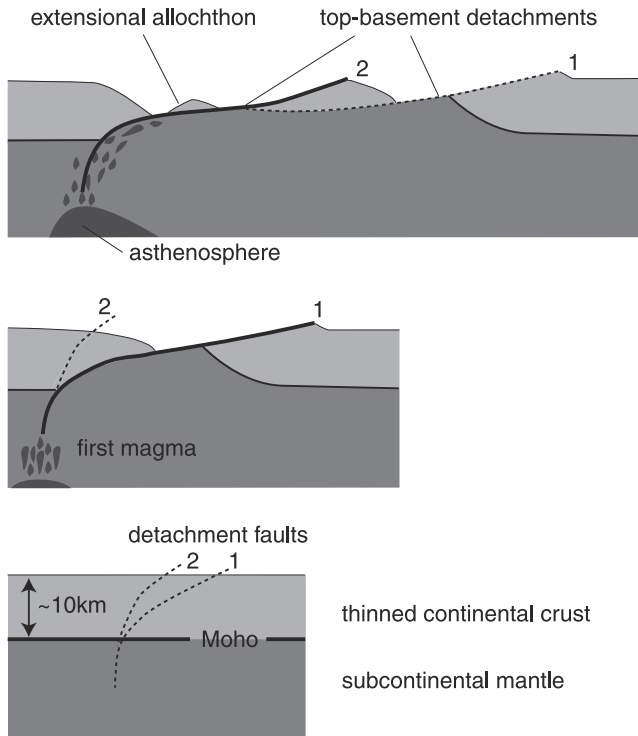


**Figure 1.** Schematic illustration of the kinematic concept of downward-concave detachment faults resulting in top-basement structures which are locally capped by extensional allochthons. Such detachments faults are thought to form during advanced rifting, when the continental crust is already thinned to about 10 km, and to lead to exhumation of subcontinental mantle.

[4] Recent interpretations of detachment structures in the Iberia Abyssal Plain which are based on reflection seismic and drill hole data suggest that rifting immediately preceding seafloor spreading is characterized by detachment faulting propagating oceanward [Manatschal *et al.*, 2001]. Manatschal *et al.* [2001] demonstrated how the mode of deformation changed from initially listric downward-convex faulting accommodating a low amount of extension to downward-concave faulting accommodating high amounts of extension. For Iberia the downward-concave faults have been interpreted indirectly, using geometric arguments [Manatschal *et al.*, 2001], but faults of similar geometry have also been predicted by numerical modeling [Lavie *et al.*, 1999]. In fact, downward-concave faults can explain the exhumation of lower crustal and subcontinental mantle rocks [Whitmarsh *et al.*, 2001] characterized by a low topographic relief, the occurrence of tectono-sedimentary breccias overlying the exhumed basement surface for square kilometers [Desmurs *et al.*, 2001], and the presence of extensional allochthons of continental origin (Figure 1). Although this process is geometrically well documented on the Lusigal 12 seismic profile across the Iberia Abyssal Plain [Beslier, 1996], the identification of top-basement detachments relies on the results of deep-sea drilling [Manatschal *et al.*, 2001]. Seismic reflections from top-basement detachment faults are

notoriously difficult to distinguish from common, i.e., non-tectonic, sediment-basement contacts. Understanding the nature of the seismic expression of top-basement detachment systems in detail is therefore crucial in order to distinguish them from nontectonic sediment-basement reflections.

[5] Exposed remnants of ancient Tethyan margins in the Alps of eastern Switzerland provide detailed 2D to 3D insights into the architecture, kinematics, and tectonic evolution of low-angle detachment structures. Studies regarding detachment faulting in the Tethyan margins predominantly focused on their architecture and evolution [e.g., Froitzheim and Eberli, 1990; Froitzheim and Manatschal, 1996; Manatschal and Nievergelt, 1997; Froitzheim and Rubatto, 1998] and comparison with present-day margins [e.g., Manatschal and Bernoulli 1999]. Recently, Hölker *et al.* [2002] investigated the seismic structure and reflectivity of detachment faults in the Iberian and Tethyan margins.

[6] In this paper, we reevaluate the architecture and kinematic evolution of the rift-related Err detachment and simulate its seismic response. The Err detachment is an outstanding example of a top-basement detachment, which is locally capped by extensional allochthons and elsewhere directly overlain by synrift and postrift sediments [Froitzheim and Eberli, 1990]. It is spectacularly exposed in the Err nappe in the Alps of eastern Switzerland (Figures 2, 3b, and 4), and has been interpreted as part of a low-angle detachment fault system cutting from the upper crust into the mantle and leading to the exhumation of subcontinental mantle within the Platta-Err OCT [Manatschal and Nievergelt, 1997]. We seek to combine the geological, tectonic, and seismic characteristics of this top-basement structure along a 14 km long upper crustal segment. In doing so, we first describe the Err detachment and discuss the kinematic concept of top-basement detachment faults. We then present a high resolution seismic velocity and density model of the Err detachment and its surroundings and evaluate the seismic response through full waveform simulation of a typical marine seismic reflection survey. The resulting synthetic CMP-stacked and time-migrated sections allow us to characterize the pertinent seismic features of the Err detachment system. We shall demonstrate that although the dimensions of the tectonic features associated with top-basement detachments are too small to be resolved deterministically in the seismic images (geological structures smaller than about one dominant seismic wavelength are not discernible as such even in perfectly migrated seismic images), they can be identified on the basis of their characteristic seismic signatures. Finally, we review the Lusigal 12 profile across the Iberia Abyssal Plain for similar seismic patterns and apply our results from the Err models to reinterpret an inferred top-basement detachment (Hobby High detachment [Manatschal *et al.*, 2001]) in the Iberia Abyssal Plain.

## 2. Geological Setting

### 2.1. Overall Situation

[7] Remnants of a Middle Jurassic rift-related detachment system, which resulted in the opening of the Liguria-Piemonte ocean, are exposed in the Platta and Err nappes

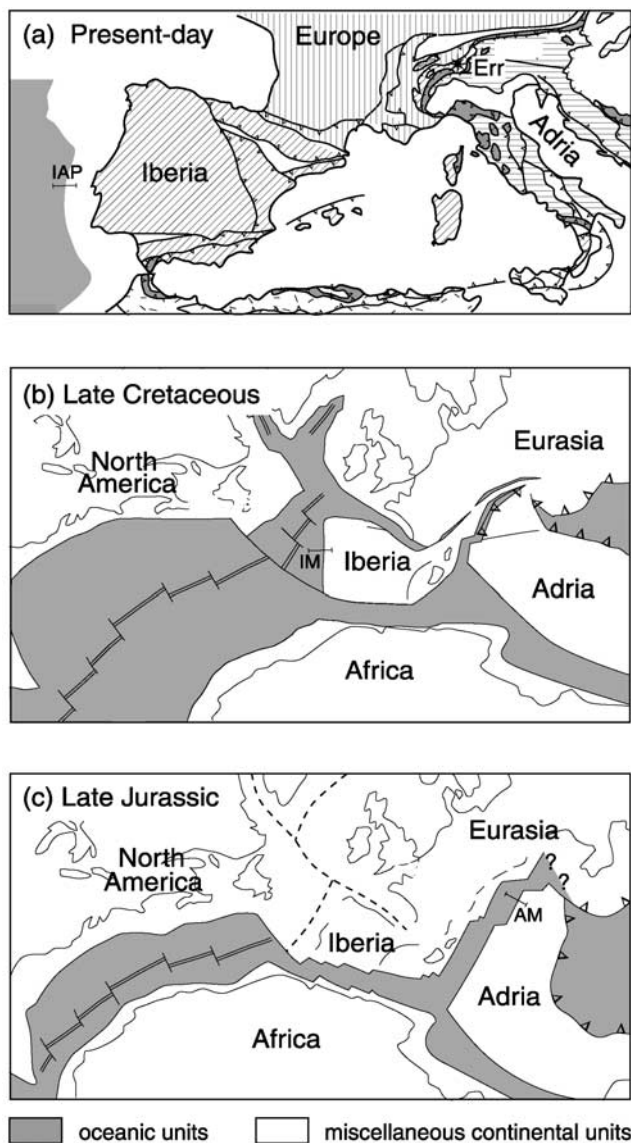


**Figure 2.** (a) Schematic tectonic map of SW Europe showing the locations of the Iberia Abyssal Plain (IAP) and the Err detachment system (Err). Paleogeographic maps for (b) the Late Cretaceous and (c) the Late Jurassic showing the tectonic framework of the corresponding Iberian margin (IM) and the Adriatic margin (AM). Modified after *Manatschal and Bernoulli* [1999].

in the Alps of Eastern Switzerland. The Platta and Err nappes preserve an ancient OCT, the Platta-Err OCT, situated in the transition between the northeastern Liguria-Piemonte ocean and the Adriatic margin (AM in Figure 2) [*Manatschal and Nievergelt*, 1997]. During Late Cretaceous convergence, this OCT has been telescoped and sampled within a west-vergent thrust stack. Extension following this first collision phase and Eocene continent-continent collision between the Adriatic and the European plates was strongly localized and affected only parts of the previously formed nappe stack [*Froitzheim et al.*, 1994]. The localized nature of Alpine

deformation and the weak metamorphic overprint, which never exceeded lowermost greenschist facies in the northern Err and Platta nappes [*Ferreiro Mählmann*, 2001], explains the excellent preservation of rift-related structures within these nappes.

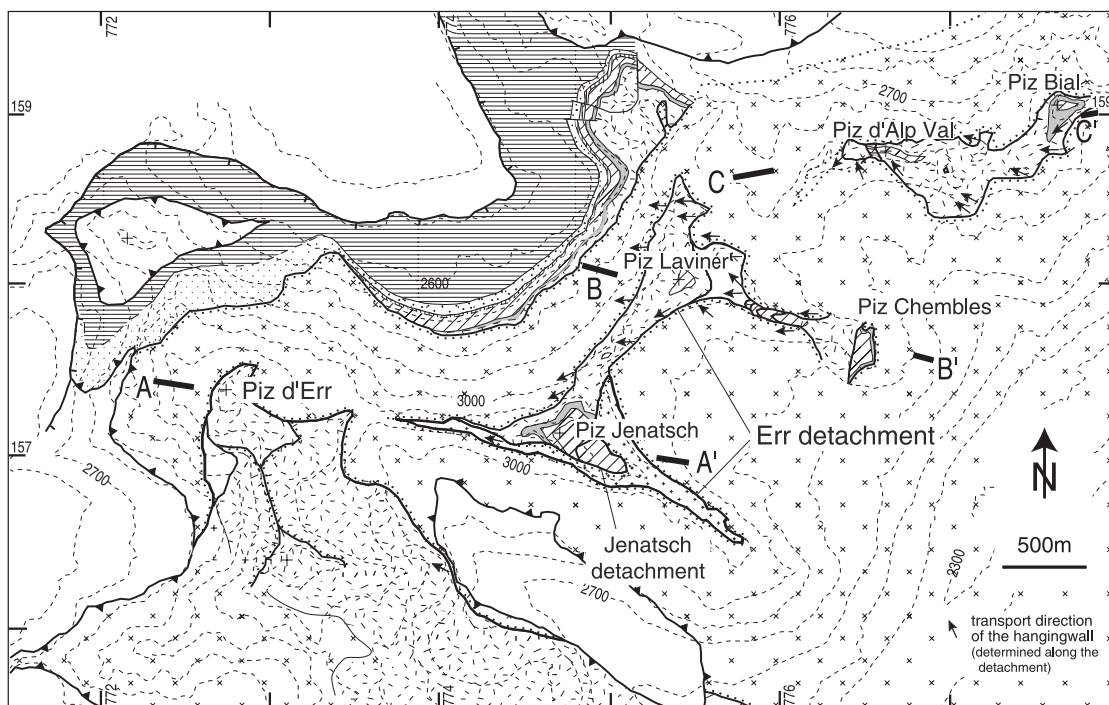
[8] The architecture of the Platta-Err OCT is controlled by a system of low-angle detachment faults [*Manatschal and Nievergelt*, 1997]. These faults are shallow crustal structures with a top-to-the-ocean sense of shear. They form breakaways in the continental crust to the east and exhumed mantle rocks to the west. Along the detachment faults, tectono-sedimentary breccias and continent-derived blocks of variable size, called extensional allochthons, overlie exhumed continental and mantle rocks, and are sealed by postrift sediments. The best preserved and most spectacular part of the detachment system is the Err detachment, which is exposed in the area of Piz d'Err-Piz Bial in the Err nappe (Figures 3 and 4).

## 2.2. Err Detachment

[9] The Err detachment was described by *Froitzheim and Eberli* [1990] and *Manatschal and Nievergelt* [1997]. Its footwall consists of massive granite and is exposed over 18 km parallel to the east-west transport direction. In the area of Piz d'Err-Piz Bial (Figure 3), the former hanging wall structure is exposed over about 6 km and preserves pre-Alpine contacts to the footwall. The hanging wall consists of tilted fault blocks of Variscan basement rocks and Triassic prerift sediments. Both the basement and the prerift sediments are systematically cut by the Err detachment and form extensional allochthons (Figures 3 and 4). The individual fault blocks are separated by high-angle faults and are of variable size ranging vertically from 50 to 250 m and horizontally from 100 to 1500 m. An incisement structure is preserved at Piz Jenatsch where a higher and older detachment fault is cut by the younger and lower Err detachment (Figure 3b).

[10] On the basis of geological mapping, a displacement of more than 10 km has been determined for the Err detachment [*Manatschal and Nievergelt*, 1997]. Dynamic recrystallization of quartz did not occur along the fault, suggesting that the fault formed under metamorphic conditions below greenschist facies (<300°C) [*Manatschal*, 1999]. The fault rocks associated with the detachment fault are 40 to 160 m thick green cataclasites, which grade downward into massive, undeformed Variscan granite. The occurrence of green cataclasites as clasts in synrift sediments indicates a rapid syntectonic healing of these fault rocks. The fault plane of the Err detachment is a sharp and a well-defined horizon marked by a characteristic black fault gouge, which accommodated most of the displacement [*Manatschal*, 1999]. Shear-sense criteria from fault rocks indicate a top-to-the-ocean sense of shear. These observations confirm that the Err detachment fault is a late, shallow crustal structure. Continentward it formed a break-away in the continental crust and penetrated oceanward into deeper crustal levels and probably into the subcontinental mantle [*Manatschal and Nievergelt*, 1997]. The relationships of the Err detachment with the synrift sediments are preserved

(a) Geological map of the Err region



(b) Cross section of the present-day situation

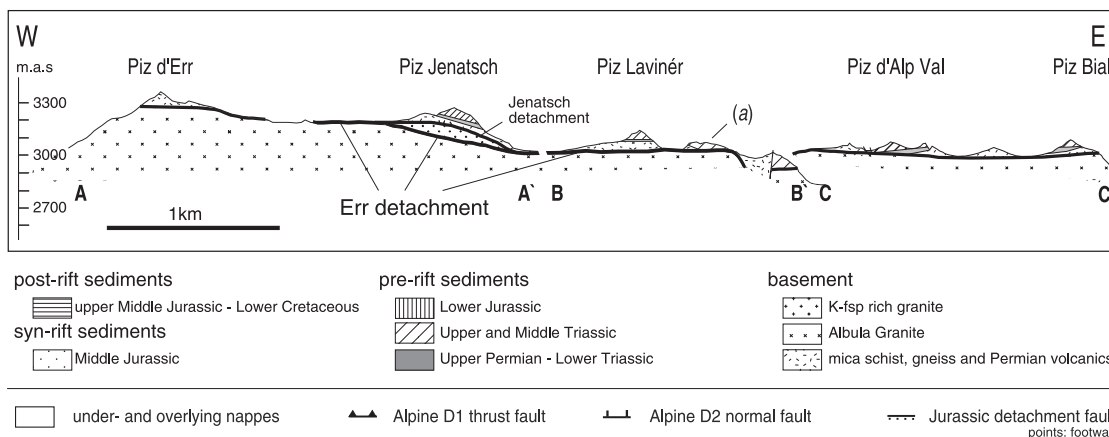


**Figure 3.** (a) Geological map of the Piz d'Err-Piz Bial area (Oberhalbstein, Alps of southeastern Switzerland). (b) Present-day cross section across the area of Piz d'Err-Piz Bial. The prominent Err detachment truncates extensional allochthons and high-angle normal faults separating these allochthons. An incisement structure is preserved at Piz Jenatsch where a higher and older detachment fault, the Jenatsch detachment, is cut by the younger and lower Err detachment. The allochthon east of Piz Lavinér, labeled (a), is that shown in Figure 4. Coordinates correspond to the CH1903 LV03 system (swiss grid). Modified after *Manatschal and Nievergelt* [1997].

outside the previously studied transect in the northwestern part of the Piz d'Err-Piz Bial area (Figure 3a) and in several other locations in the Err nappe [Manatschal and Nievergelt, 1997]. There synrift sediments stratigraphically overlie basement, prerift sediments, and also the Err detachment (e.g., north of Piz d'Err in Figure 3a). Exhumation of the Err

detachment to the seafloor is corroborated by the occurrence of clasts of the green cataclasites and of indurated black fault gouges in synrift deep-marine breccias [Froitzheim and Eberli, 1990; Manatschal and Nievergelt, 1997].

[11] The small angles ( $<20^\circ$ ) observed between the synrift sediments and the detachment surface confirm that the Err

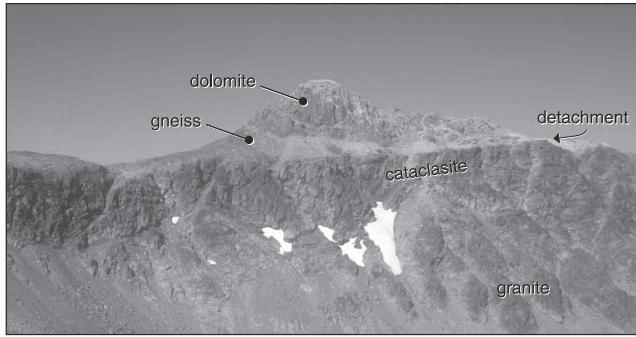


**Figure 4.** The low-angle Err detachment fault juxtaposing Variscan continental basement (granite) in the footwall against Variscan gneiss and Triassic prerift sediments (mostly dolomite) in the hanging wall. The footwall consists of a 150 m thick cataclastic zone, grading downward into Variscan granite. View from the South onto Peak 3059 east of Piz Lavinér (corresponding to label *a* in Figure 3).

detachment was a subhorizontal structure, of which no longer-active segments were exhumed to the seafloor and formed a so-called top-basement detachment. Previous studies considered local remnants of the former hanging wall, so-called extensional allochthons, to represent the hanging wall of a shallow intra-basement detachment [Froitzheim and Eberli, 1990; Manatschal and Nievergelt, 1997].

[12] The postrift sediments locally overlie prerift sediments of extensional allochthons or rest directly on the exhumed detachment fault. In the area north of Piz d'Err, the synrift breccias are directly overlain by hemipelagic shales and pelagic or turbiditic limestones (Early Cretaceous Palombini formation), whereas further to the north the same breccias are overlain by middle to late Jurassic radiolarites which pass upward into the Palombini formation. The lower part of the Palombini formation includes submarine mass-flow deposits yielding clasts derived from the prerift and synrift sediments and also from the basement. This suggests that the submarine relief created by the extensional allochthons persisted over tens of million years and was only buried during Early Cretaceous.

### 2.3. Kinematic Model

[13] On the basis of geometric reconstructions and kinematic data, Manatschal and Nievergelt [1997] proposed that a progressive warping of the initially listric detachment faults and the inactivation of older breakaways lead to a migration of detachment faulting toward the future ocean. This kinematic model was strongly influenced by models developed for the metamorphic core complexes of the southwestern United States [cf. Lister and Davis, 1989]. New data from the Platta-Err OCT and new kinematic models for mantle exhumation developed in the Iberia Abyssal Plain show that the original model has to be revised. Recently, Manatschal et al. [2001] proposed a model for the evolution of detachment faults during the latest stages of rifting. This model is based on the kinematic inversion of interpreted depth-migrated seismic profiles and drill hole

data from ODP Legs 149 and 173. Manatschal et al. [2001] demonstrated that following initial thinning of the crust to less than 10 km, new faults propagated toward the future ocean. Associated with this late faulting is a change in the mode of deformation from initially downward-convex to finally downward-concave listric faulting leading to a kinematic situation in which the footwall was pulled out from underneath a relatively stable hanging wall and was exposed over tens of kilometers at the seafloor (Figure 1). This model is similar to the rolling hinge model [Buck, 1988] and is also consistent with numerical models [Lavie et al., 1999]. It explains how faults can accommodate large offsets, which lead to the exhumation of crustal and mantle rocks to the seafloor within an OCT without producing a major submarine relief. In this model, the extensional allochthons are interpreted as remnants of a former hanging wall block which became disconnected and were transported as passive blocks on the footwall, a situation like on a conveyor belt.

## 3. Seismic Models of the Err Detachment

### 3.1. Reconstruction of the Architecture of the Err Detachment

[14] In order to compare the seismic response of the Err detachment with that from top-basement detachment faults from present-day margins (e.g., HHD as interpreted by Manatschal et al. [2001]) and to generalize the results for top-basement detachment faults elsewhere, we have to reconstruct the pre-Alpine situation of the Err detachment. Our reconstruction is entirely based on evidence from geological mapping.

#### 3.1.1. Err Detachment and Its Footwall

[15] The Err detachment is an overall horizontal structure along the central part of the reconstructed profile ( $x = 2000$  to  $10000$  m in Figure 5). Depth variations shown in the reconstruction correspond to present-day variations in altitude.

[16] The footwall of the Err detachment consists of green cataclasite grading downward into undeformed granite. The thickness of this damaged zone is defined as the vertical distance from the fault plane to the uppermost undeformed granite. We simulated the lateral thickness variations ( $100 \pm 20$  m) of this damaged zone by means of a stochastic data sequence characterized by a Gaussian probability distribution and exponential covariance function. The structure of the basement forming the deeper footwall ( $>300$  m below the detachment) is simplified in the reconstruction. We believe that the basement was affected by deeper detachment structures which were reactivated by Alpine thrust faults, but which we are not able to reconstruct. For this reason, we consider the reconstruction of the basement in Figure 5 to be adequate down to approximately 6000 m.

#### 3.1.2. Extensional Allochthons

[17] In contrast to the footwall, the extensional allochthons forming the hanging wall have been partly eroded. However, mapping and projection into the section allows for a reliable reconstruction of the lithological composition and of the high-

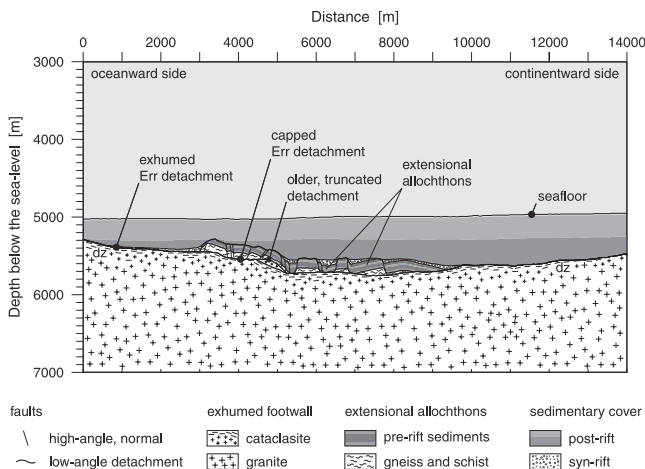


**Figure 5.** Geological reconstruction of the Err detachment for a postrift stage before the onset of Alpine convergence. The Err detachment fault exhumed its footwall over large distances to the seafloor. The uppermost footwall is cataclastically deformed ( $dz =$  damaged zone). Locally, the detachment is capped by extensional allochthons. With regard to the seismic response of the detachment we distinguish between the capped and exhumed segments. Vertical exaggeration: 2x.

angle faults separating the extensional allochthons. We have reconstructed the hanging wall geometries along three transects which were then put together (Figure 3) and which form the central segment of the reconstruction ( $x = 2000$  to  $10000$  m in Figure 5). The high-angle faults (Figure 5) are either observed in the field or introduced in order to maintain the observed style of deformation and formation thicknesses observed in adjacent preserved blocks.

[18] Because of erosion, the pre-Alpine thickness of the allochthons cannot be reconstructed. Only the minimum and maximum thicknesses are known from the present-day situation and the regional stratigraphy. We assume that little synrift erosion has taken place. This is justified by the fact that the hanging wall was never exposed above sea level and by the relatively small volume of synrift clastic sediments. Erosion occurred only at the top of the extensional allochthons and along fault scarps. Hence the shown 2D geometry of the synrift unconformity is somewhat speculative. However, a larger or smaller thickness within the given limits would not fundamentally change the seismic expression of the allochthons.

### 3.1.3. Synrift Sediments

[19] Synrift sediments (Middle Jurassic Saluver Group) occur only locally along the transect. They overlie the allochthons, and their depositional geometry suggests that their deposition partly predates the Err detachment. However, the occurrence of clasts of green cataclasites and black gouge typically associated with the Err detachment within higher levels of the synrift sediments clearly indicate that the youngest parts of the synrift sediments have been deposited while the Err detachment was active.

### 3.1.4. Postrift Sediments

[20] The postrift succession of the Err nappe consists of a pelagic to hemipelagic sequence of radiolarian cherts, limestones and shales which locally onlap onto the allochthons forming the hanging wall. For our models we simplified the sedimentary cover assuming a lower partially lithified formation and an upper entirely unconsolidated formation. The total thickness of the postrift succession in the reconstruction is broadly twice the present-day thickness assuming an original porosity of about 40 to 60%.

### 3.1.5. Extrapolation

[21] We have extended the reconstruction of the Err detachment 2 km oceanward and 4 km continentward from the central part of the reconstruction. On the oceanward side, the Err detachment was exhumed. Its rise at  $x < 2000$  m is supported by the onlap of the sedimentary cover which can be observed in the field. Conversely, the reconstruction of the Err detachment on the continentward side is somewhat speculative, but is consistent with all available evidence.

### 3.2. Model of the Seismic Structure

[22] To quantify the seismic structure (Figure 6), we construct 2-dimensional P wave velocity  $V(x, z)$  and bulk density  $\rho(x, z)$  models. The models consist of three components representing different spatial scales: (1) the geological/geometrical model (Figure 5), (2) the large-scale velocity-depth and density-depth trends of each lithological unit, and (3) the small-scale velocity fluctuations of each lithological unit. The first two components are described deterministically and are based on field observations and laboratory measurements. Conversely, we use a stochastic approach to represent the small-scale velocity fluctuations [e.g., Frankel and Clayton, 1986; Holliger et al., 1993; Holliger and Levander, 1994]. Our primary motivation for this approach is the observation that sonic logs are characterized by prominent small-scale velocity fluctuations, which make up 5 to 10% of the underlying large-scale velocity-depth function [Holliger, 1996]. Because of this inherent local variability of seismic velocity distribution, an exclusively deterministic characterization of seismic models is generally inadequate. Descriptions of the stochastic method are given by Goff and Jordan [1988], Holliger [1996], Dolan et al. [1998], and Goff and Jennings [1999]. These local variations of the seismic velocity can have a profound effect on the propagation of seismic signals. In fact, much of what is frequently perceived as “background noise” in seismic reflection data corresponds to primary seismic energy scattered from local, small-scale velocity fluctuations [Holliger, 1997; Martini et al., 2001]. We therefore believe that the careful representation of the stochastic model components, contributes significantly to the overall high degree of realism of our synthetic seismograms and their comparability to observed data from similar tectonic environments.

[23] Table 1 lists the velocity-depth and density-depth trends and the statistical characterizations of velocity fluctuations of each lithological unit. This summary is based on analyses presented by Hölker et al. [2002]. The velocity and

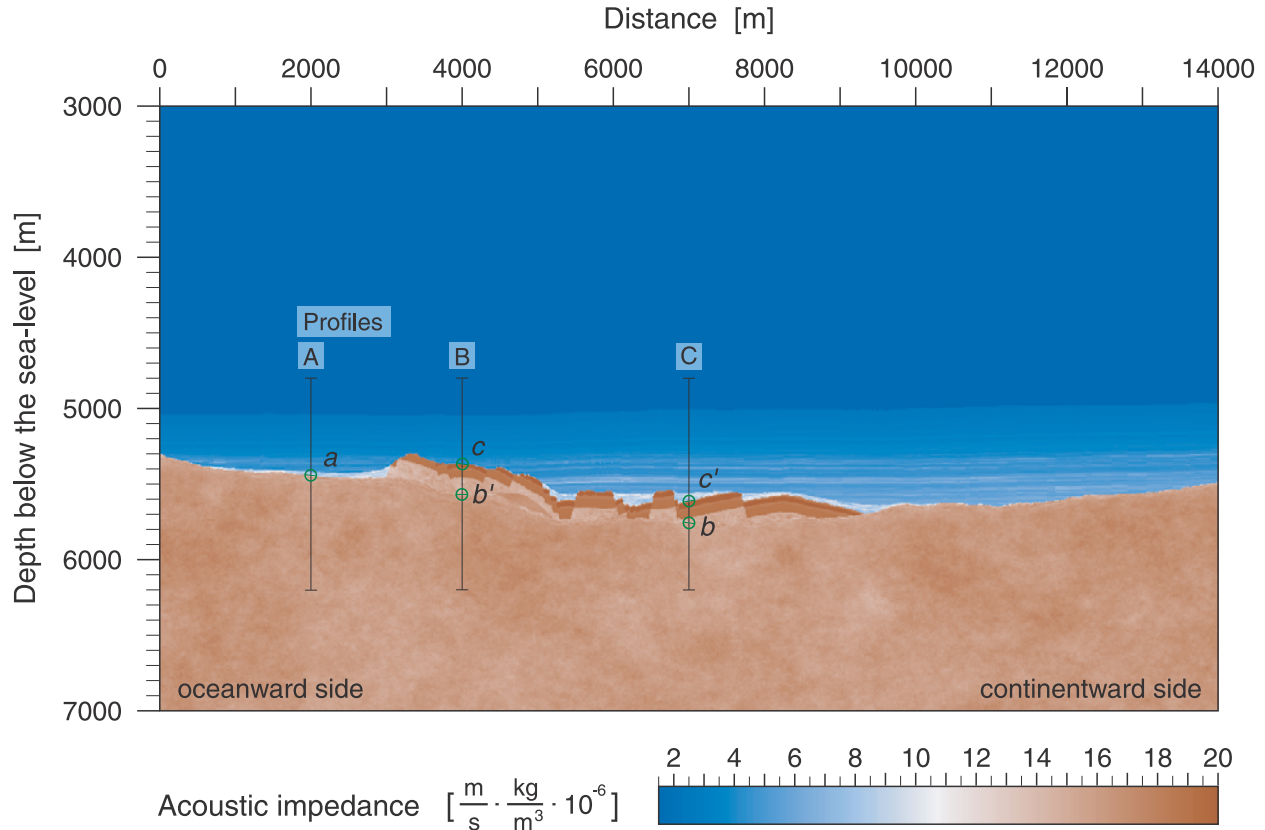


**Figure 6.** Seismic structure of the Err detachment system in terms of its acoustic impedance. Green circles denote interfaces crucial for the subsequent interpretation of the corresponding seismic response: (*a*) the exhumed detachment forming a contact of sediment to tectonized basement, (*b* and *b'*) the detachment overlain by allochthons, (*c*) the contact of unconsolidated postrift sediments with the nontectonic top of an allochthon, and (*c'*) the contact of moderately lithified early synrift sediments with the nontectonic top of an allochthon. The vertical profiles (A to C) refer to the later discussion of the seismic response. Vertical exaggeration: 2x.

density structures of each lithological unit were modeled separately and were finally assembled according to the geometrical model. In doing so, we generally neglect density fluctuations, since they are considered to be strongly correlated with velocity fluctuations. Moreover, we neglected velocity fluctuations in the prerift sediments, because the thickness of this unit corresponds only to about 1/25–1/3 of the dominant seismic wavelength. Special attention was paid to the simulation of the more complex velocity structure of the footwall of the Err detachment, where a transition from cataclasites at the top to undeformed granite 40 to 160 m below must be realized. We modeled the velocity structure of both the cataclasite and the granite separately and superimposed them according to a weight function, which defines the relative proportions as a function of distance from the detachment fault [Hölker *et al.*, 2002].

### 3.3. Seismic Modeling and Processing

[24] Synthetic CMP-stacked and time-migrated seismic sections were generated by computing individual shot-

gathers and subsequent standard reflection seismic processing. The seismic modeling was based on a finite-difference solution of the 2D acoustic wave equation [sufdmod2 from Cohen and Stockwell, 2000]. This approach considers all scattered and multiple acoustic waves, cylindrical spreading, as well as acquisitional and processing effects.

[25] The source signal is a Ricker wavelet with a peak frequency of 35 Hz. The spatial discretization interval was 2 m, which yields at least 10 grid points per minimum wavelength. Each shot-gather is simulated in a segment of the seismic model comprising the streamer length plus a buffer zone of 240 m on both sides. Together with absorbing boundary conditions, the buffer zones attenuate the impact of artificial edge reflections. A total number of 272 shots with a single side 77 channel receiver array pointing oceanward were modeled. The design of the simulated surveys emulates that of common marine seismic reflection surveys (Table 2), except for the water depth which we decreased to 2000 m in order to keep grid dispersion [e.g., Alford *et al.*, 1974; Kelly *et al.*, 1976] under control. Firstly, this resulted

**Table 1.** Parameters of the Velocity and Density Models<sup>a</sup>

| Lithological Unit      |                                  | Velocity, m/s | Density, kg/m <sup>3</sup> | Velocity Fluctuations <sup>b</sup> |           |       |                  |
|------------------------|----------------------------------|---------------|----------------------------|------------------------------------|-----------|-------|------------------|
|                        |                                  |               |                            | $a_x$ , m                          | $a_z$ , m | $\nu$ | $\sigma_V$ , m/s |
| Sed. cover             | upper postrift <sup>c</sup>      | $z + 1530$    | $1.4z + 1600$              | 10000                              | 2         | 0.3   | $0.3z + 10$      |
|                        | lower postrift <sup>c</sup>      | $z + 1700$    | $1.4z + 1600$              | 3000                               | 5         | 0.18  | see <sup>h</sup> |
|                        | synrift                          | 3500          | 2500                       | 100                                | 3         | 0.2   | 400              |
| Allochthons (pre-rift) | Agnelli formation <sup>de</sup>  | 6010          | 2700                       | -                                  | -         | -     | -                |
|                        | Kössen formation <sup>de</sup>   | 6388          | 2720                       | -                                  | -         | -     | -                |
|                        | Hauptdolomite <sup>df</sup>      | 6706          | 2840                       | -                                  | -         | -     | -                |
|                        | Raibl Group <sup>df</sup>        | 6347          | 2720                       | -                                  | -         | -     | -                |
|                        | Buffalora Group <sup>df</sup>    | 6453          | 2750                       | -                                  | -         | -     | -                |
|                        | Fuorn formation <sup>dg</sup>    | 5387          | 2670                       | -                                  | -         | -     | -                |
|                        | Chazfora formation <sup>dg</sup> | 5364          | 2650                       | -                                  | -         | -     | -                |
| (basement) Footwall    | gneiss & schist                  | 5345          | 2710                       | 160                                | 40        | 0.14  | 300              |
|                        | cataclasite                      | 5385          | 2680                       | 40                                 | 2         | 0.1   | 374              |
|                        | granite                          | 5780          | 2680                       | 600                                | 400       | 0.13  | 180              |

<sup>a</sup>For the underlying analyses of the velocity-depth and density-depth trends and the velocity fluctuations we refer to *Hölker et al.* [2002]. The  $z$  in this table generally refers to depth below the seafloor, specified in meters.

<sup>b</sup>Described statistically using the *von Kármán* [1948] model [e.g., *Holliger*, 1996] and quantified by a horizontal correlation length  $a_x$ , a vertical correlation length  $a_z$ , a parameter  $\nu$  related to the fractal dimension of the process, and  $\sigma_V$  the standard deviation of velocity.

<sup>c</sup>Postrift lithologies in the Err domain are radiolarite, pelagic limestone and shales. For modeling we use the properties of a totally unconsolidated upper unit and a partially consolidated lower sedimentary unit.

<sup>d</sup>See *Furrer et al.* [1985] for the geology of that formation.

<sup>e</sup>Predominantly limestones.

<sup>f</sup>Triassic dolomites.

<sup>g</sup>Permian to Triassic sandstones.

<sup>h</sup>Lognormal distribution of  $\Delta V$  with  $\mu_y = 5.7$  and  $\sigma_y = 0.6$ , shifted by  $-300$  m/s.

in an increased curvature of diffractions. This is undesirable, but it does not affect our entirely qualitative interpretation of diffraction effects. Secondly, to match the spectrum of incidence angles of Lusigal 12, we had to accept a somewhat lower subsurface coverage in the simulated Err survey (Table 2), which does not have any detrimental effects on the seismic imaging of the targeted geological features. The resulting synthetic shot-records were processed as outlined in Table 3 resulting in the sections shown in Figure 7.

**Table 2.** Design of the Simulated Err and the Real Lusigal 12 Surveys

| Parameter                       | Err                  | Lusigal 12 <sup>a</sup> |
|---------------------------------|----------------------|-------------------------|
| Water depth                     | 2020 m <sup>b</sup>  | 5030 m                  |
| Source depth                    | 20 m                 |                         |
| Receiver depth                  | 0 m                  |                         |
| Dominant frequency              | 35 Hz                | 24 and 45 Hz            |
| Maximum frequency               | 70 Hz                | 64 Hz                   |
| Source signal                   | Ricker               | mixed phase             |
| Shot point interval             | 48 m                 | 50 m                    |
| Receiver interval               | 24 m                 | 25 m                    |
| CMP interval                    | 12 m                 | 12.5 m                  |
| Maximum offset                  | 1872 m <sup>d</sup>  | 2700 m                  |
| Incidence spectrum <sup>c</sup> | $0.3-25^{\text{od}}$ | $1.7-15^{\circ}$        |
| Maximum coverage                | $20^{\text{d}}$      | 24                      |

<sup>a</sup>*Beslier* [1996].

<sup>b</sup>Water depth when modeling the shot gathers. In all Figures, 3000 m respectively 4 s travel time were added to the annotations to represent a realistic water depth of the Err system.

<sup>c</sup>Angles of incidence with respect to the seafloor.

<sup>d</sup>In order to match the angular spectrum of the Lusigal 12 profile, the maximum offset in the Err data was limited to 1200 m resulting in a incidence spectrum of  $0.3-16^{\circ}$  in the profiles shown in Figure 7. In doing so, the subsurface coverage was reduced to 12.

### 3.4. Seismic Response

[26] We first discuss the seismic structure and response of the footwall of the Err detachment and then the structure and response of the interfaces which are crucial for the geological interpretation. These interfaces are the exhumed and the capped segments of the Err detachment (Figure 5) as well as the top of the extensional allochthons capping the detachment. Figure 6 shows the seismic structure of the Err detachment in terms of the acoustic impedance, i.e.,  $V(x, z) \cdot \rho(x, z)$ , Figure 7 shows the corresponding seismic response, and in Figure 8 we look at the details of the crucial interfaces (labeled  $a$  to  $c$ ) by means of selected 1D profiles.

#### 3.4.1. Footwall of the Err Detachment

[27] The shallow footwall of the Err detachment consists of a cataclasite, i.e., a damaged zone, grading downward

**Table 3.** Processing Sequence for the Simulated Err Survey

| Processing Tasks                                  |
|---|
| 1. Assignment of the geometry data                |
| 2. band-pass filter, 4–8–50–70 Hz                 |
| 3. sort to CMP gathers                            |
| 4. velocity analysis on 8 CMP gathers             |
| 5. normal moveout correction                      |
| 6. near offset 12 fold CMP stack                  |
| 7. Gazdag phase-shift time migration <sup>a</sup> |
| 8. band-pass filter, 4–8–50–70 Hz                 |
| 9. AGC <sup>b</sup> , window length 2 s           |

<sup>a</sup>Interval velocity depth function for migration was computed from the input velocity model by taking horizontal averages.

<sup>b</sup>AGC using Gaussian taper and normalization with respect to the entire stack, in order to preserve lateral amplitude variations.

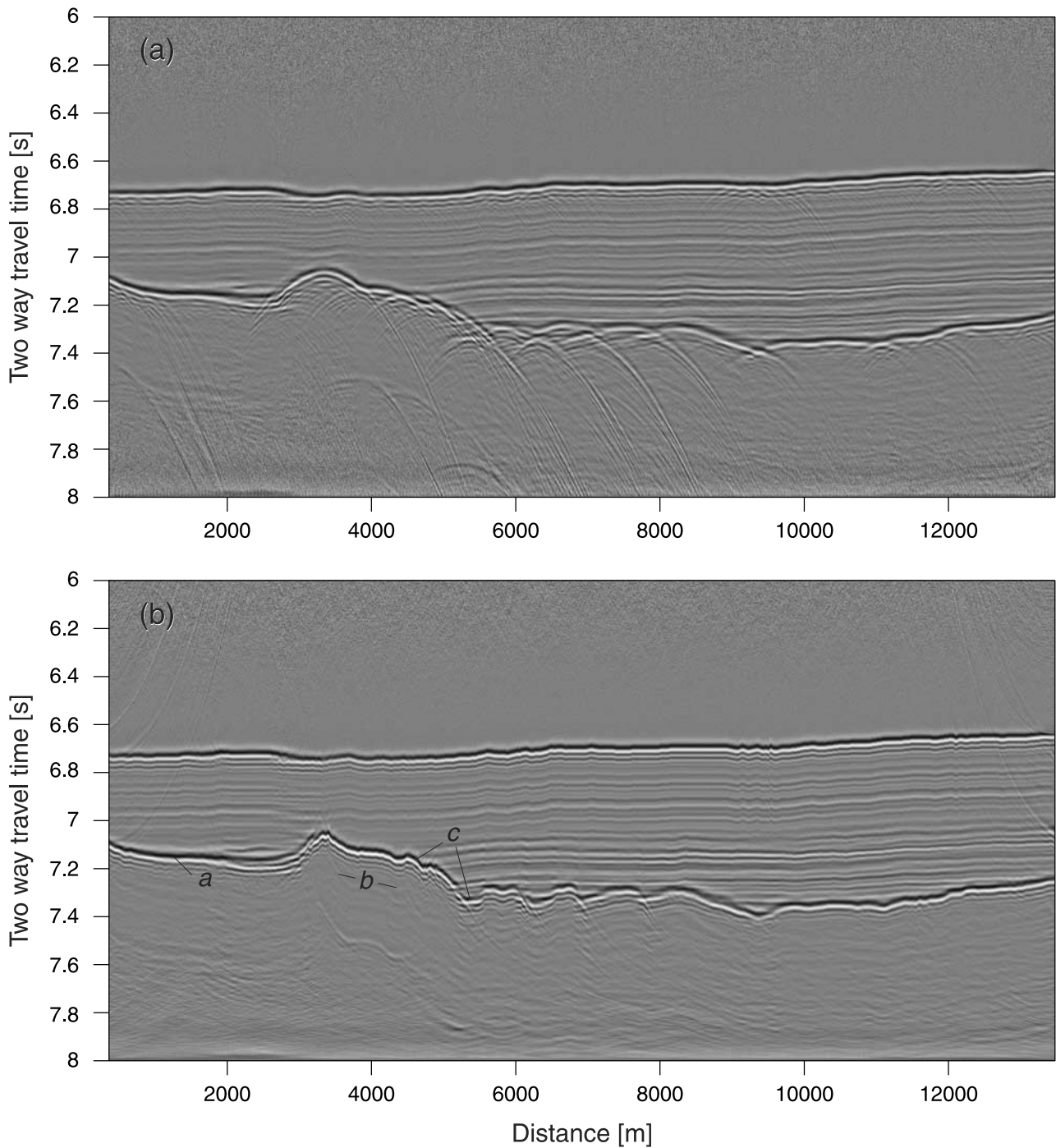


**Figure 7.** Synthetic seismic profiles of the Err detachment for the geological model shown in Figure 5 and the corresponding seismic structure shown in Figure 6: (a) CMP-stacked and (b) time-migrated sections. The exhumed Err detachment is characteristically imaged by a very continuous reflection of constant amplitude (label *a*). In contrast, the capped detachment (label *b*) is seismically transparent. However, it can be interpreted on the basis of the characteristic seismic response of the associated extensional allochthons. The tops of these allochthons give rise of individual strong diffractions in the stacked section and are imaged by strong, broken up reflections of variable amplitude in the migrated section (label *c*).

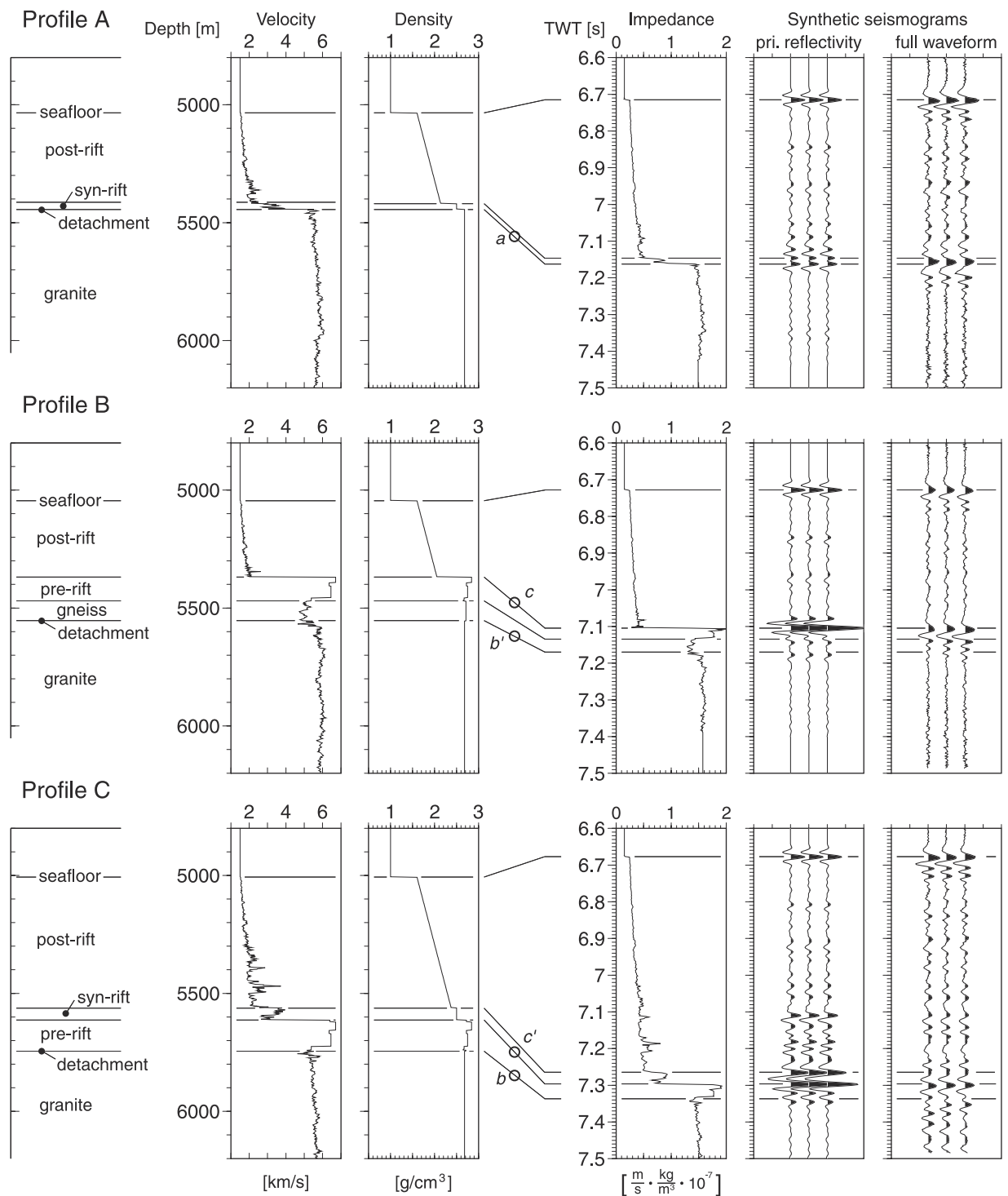


**Figure 8.** Seismic structure and response of crucial interfaces. The profiles and interface-labels correspond to those in Figures 6 and 7. The velocity and density structures are given as functions of depth, whereas the impedance profile is converted to two-way-travel time (TWT). The synthetic seismograms marked as “pri. reflectivity” are based on reflection coefficient sequences convolved with a Ricker wavelet with a center frequency of 35 Hz. The seismograms denoted as “full waveform” are extracted at corresponding locations from the time-migrated section shown in Figure 7b. See text for a discussion of the particular interfaces.

into granite. Although the small-scale velocity fluctuations of the cataclasite and the undeformed granite show different characteristics, the seismic structure at scales of a dominant wavelength is quite homogeneous due to fast syntectonic fracture healing in the fault rocks [Hölker *et al.*, 2002]. As opposed to detachment faults cutting through exhumed mantle rocks, there is no low-velocity zone associated with the damaged zone below the Err detachment and hence there is no seismic response from this homogeneous footwall [Hölker *et al.*, 2002].

### 3.4.2. Exhumed Err Detachment

[28] Where the Err detachment was exhumed to the seafloor (label *a* in Figures 6, 7, and 8) and where it is overlain by synrift or postrift sediments, it generally represents a slow-to-fast interface and hence is imaged by a prominent, continuous reflection of positive polarity. Because of the homogeneous velocity structure of the footwall, the only variations in amplitude are due to differences in lithification of the overlying sediments. The amplitude of the reflection is stronger where unconsolidated postrift sediments directly cover the fault ( $x < 2000$  m in Figures 6 and 7) and it is weaker where lithified synrift sediments are intercalated ( $x = 2000$  to 2700 m). Given the homogeneous velocity structure of the footwall, there are no seismic attributes associated with this sediment-basement reflection that would allow one to distinguish this top-basement detachment from a nontectonic sediment-basement contact.

### 3.4.3. Capped Err Detachment

[29] Where extensional allochthons overlie the Err detachment (label *b* in Figures 6 and 8) two configurations of the seismic interface occur. Where the cataclastic footwall is juxtaposed against a hanging wall of calcareous or dolomitic prerift sediments we observe a moderate fast-to-slow interface and hence a weak reflection of inverse polarity (label *b* in Figures 6 and 8). Where the footwall is juxtaposed against schist and gneiss in the hanging wall there is either no velocity contrast or only a very minor slow-to-fast contrast and hence no discernible seismic response (label *b'*). The 2D seismic profiles indicate that, despite its prominent structural nature, the capped Err detachment ( $x = 3000$  to 9000 m) is seismically transparent (Figure 4 and label *b* in Figure 7).

### 3.4.4. Top of the Extensional Allochthons

[30] The upper parts of the extensional allochthons consist of dolomite and limestone, which are well lithified and have high velocities and densities. Therefore they form very strong impedance contrasts with respect to the overlying synrift or postrift sediments and give rise to strong reflections. The actual strength of the reflection varies depending on whether unconsolidated postrift sediments (label *c*) or somewhat lithified synrift sediments (label *c'*) overlie the allochthons. The crucial part of their seismic response are, however, the prominent diffractions in the CMP-stack ( $x = 3000$  to 9000 m in Figure 7a). They originate from the displaced top of the allochthons where high-angle faults are emerging. The corresponding response in the time-migrated

section is a laterally discontinuous and broken up sediment-basement reflection (Figure 7b). The seismic fingerprint of the relatively small (0 to 2 dominant wavelengths) extensional allochthons is thus the strongest seismic evidence for the existence of a top-basement detachment fault.

## 4. Lusigal 12 Profile Across the Iberia Abyssal Plain

[31] The Iberia Abyssal Plain offshore Portugal (Figure 2) is one of the best studied OCT zones in magma-poor margins [Whitmarsh *et al.*, 2000]. A dense network of seismic reflection profiles has been recorded. In the following, we review a segment of the Lusigal 12 seismic profile (shot points 3970 to 4250 from Beslier [1996]; Whitmarsh and Wallace [2001]; Manatschal *et al.* [2001]) continentward of Hobby High (ODP Sites 1067 and 1068 from Whitmarsh *et al.* [1998]), whose seismic signature is similar to that of the synthetic seismic profiles across the Err detachment.

### 4.1. Observations Continentward of Hobby High

[32] Within a 3 km segment continentward of Hobby High, the Hobby High detachment (Figure 9) is exhumed and hence represents the sediment-basement contact. It is imaged as a continuous reflection (label *a* in Figure 9). Further to the east ( $x = 7$  to 10 km and  $x = 11$  to 13 km in Figure 9) the sediment-basement contact is imaged by a strong, broken up, and laterally discontinuous reflector, which is characterized by several strong diffractions in the CMP-stack (label *c* in Figure 9). The amplitudes of the response from this displaced sediment-basement reflector (label *c*) are significantly stronger than those from the continuous sediment-basement reflector oceanward (label *a*). There is no seismic response from below the broken up reflector (label *c*). This seismic signature strongly resembles that observed in the synthetic seismic data from the Err detachment (Figure 7). Continentward of Hobby High, at  $x = 10$  to 11 km (label *d* in Figure 9), a seismic signature of the top of the basement is observed which does not occur in the Err models. The top of the basement is imaged neither by a continuous nor by a broken up reflection, but appears to be somewhat transparent.

### 4.2. Reinterpretation of the Lusigal 12 Profile East of Hobby High

[33] The seismic fingerprint of the sediment-basement contact continentward of Hobby High (Figure 9), which Manatschal *et al.* [2001] interpreted as a top-basement detachment, is largely identical to that of the Err detachment (Figure 7). In the following, we shall reinterpret this segment of Lusigal 12 based on the inferred architecture of the Err detachment.

[34] This approach allows us to identify small extensional allochthons (label *c* in Figure 10) and to identify the exhumed and the capped segments of the Hobby High detachment (= HHD, labels *a* and *b* in Figure 10). The existence of small extensional allochthons is also supported by the observation of different amplitudes of the laterally continuous (label *a*) and the broken up (label *c*) top-

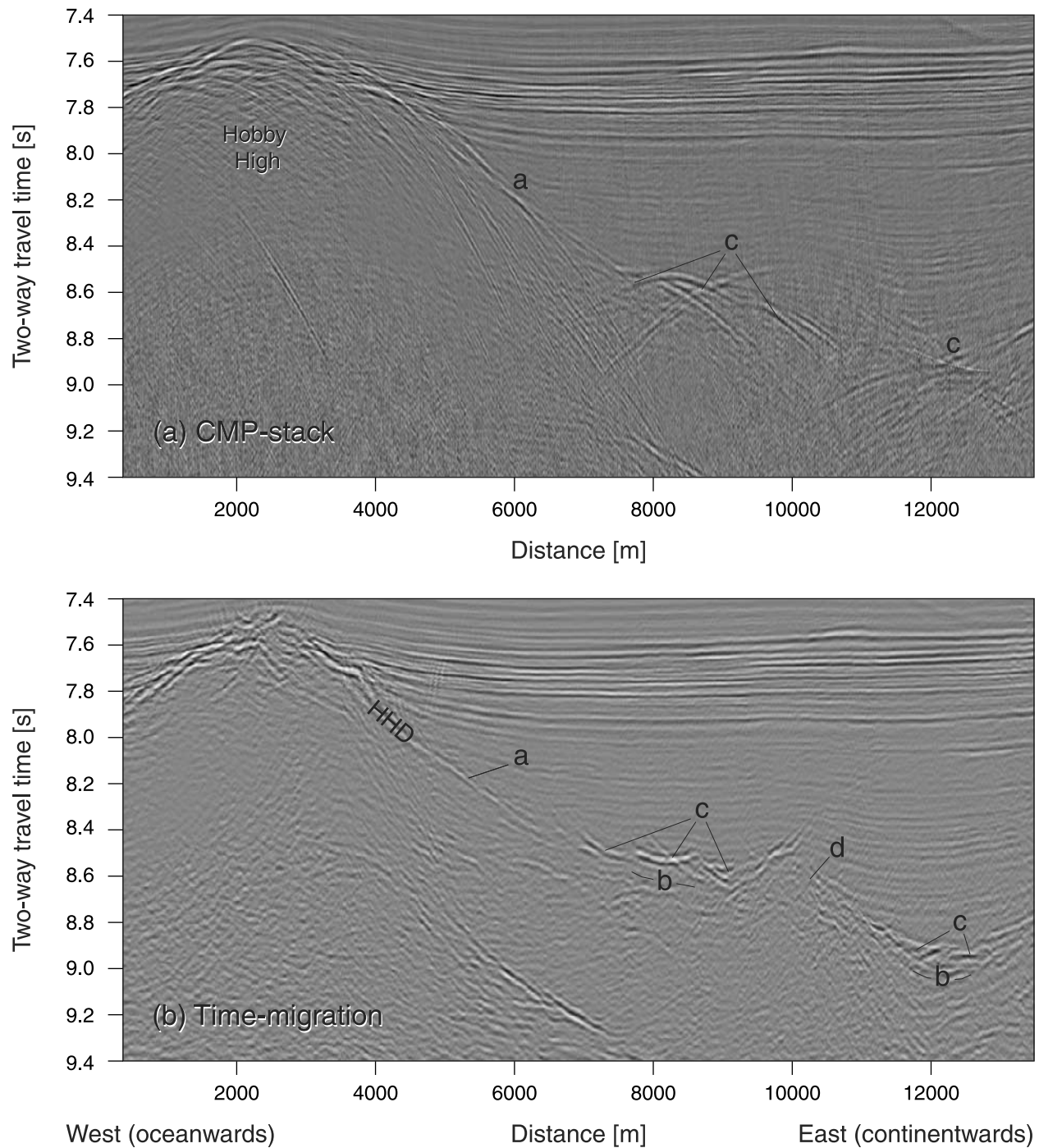


**Figure 9.** Detail of the Lusigal 12 seismic profile (processed by C. M. Krawczyk, courtesy of Geomar, Kiel) across the Iberia Abyssal Plain showing a 14 km transect east of Hobby High (shot points 3970 to 4250 from *Beslier [1996]*, *Whitmarsh and Wallace [2001]*): (a) CMP stack and (b) time-migrated section. The reflection interpreted as the Hobby High detachment (HHD) by *Manatschal et al. [2001]* has seismic features strikingly similar to the modeled seismic expression of the Err detachment (Figure 7). The segment labeled *a* shows a very continuous reflection of relatively constant amplitude. Two other segments labeled *c* show striking diffractions in the CMP stack and corresponding shifted and strong reflections of variable amplitude which have a characteristically transparent footwall (label *b*). The segment labeled *d* has no equivalent in the Err models.

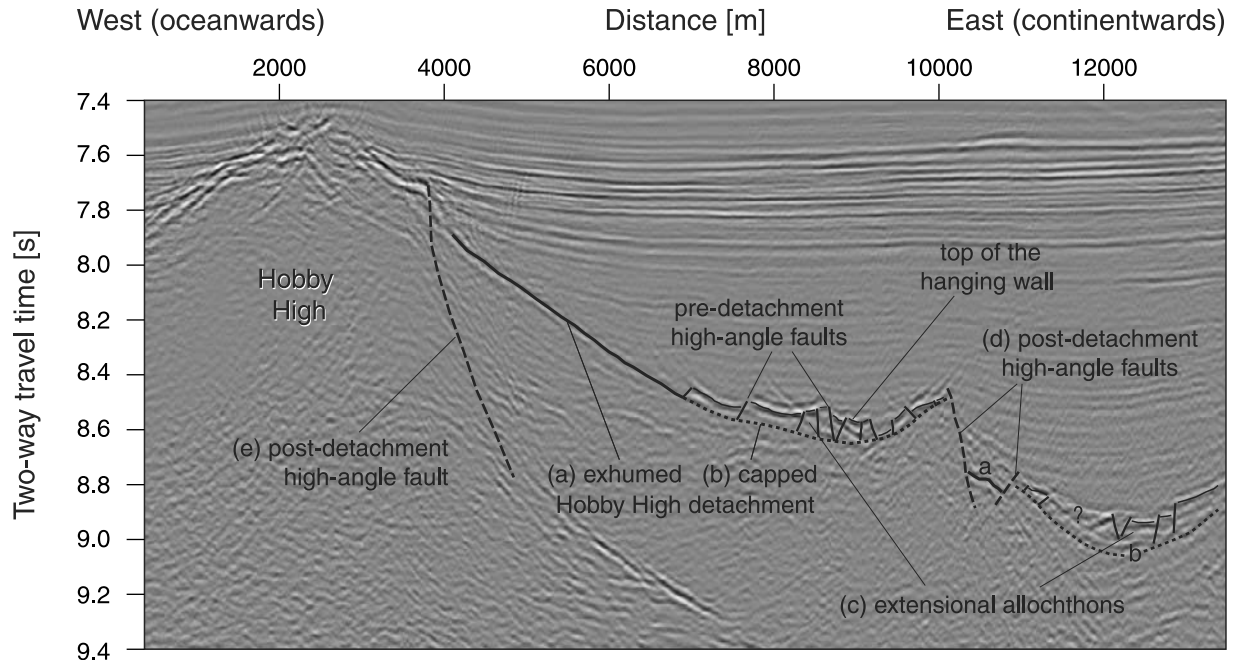


**Figure 10.** Refinement of the interpretation of the Hobby High detachment east of Hobby High. On the basis of their seismic characteristics, we identify extensional allochthons (label *c*) and after this the exhumed and the capped segments of the detachment can be recognized (labels *a* and *b*). The segment labeled *d* can be interpreted as a post-detachment graben structure. Such a postbreakup extensional structure is in line with the high-angle normal fault on the east-flank of Hobby High (label *e*) which was suggested by *Whitmarsh et al.* [2000].

basement reflection, which suggests that these reflections do not originate from the same lithological interface. The segment labeled *d* in Figure 9, which does not fit into the pattern of exhumed and capped detachments, is interpreted as a post-detachment graben structure (label *d* in Figure 10). We therefore postulate the existence of high-angle normal faults cutting across the latest low-angle detachment fault. Such a post-detachment normal fault has indeed been proposed by *Whitmarsh et al.* [2000] at the continentward flank of Hobby High (label *e* in Figure 10). The onlap of the entire sedimentary cover onto these late high-angle faults implies that all sediments observed in this seismic section are indeed of post-detachment age as suggested by *Wilson et al.* [2001]. *Manatschal et al.* [2001] interpreted the structure at location *d* (Figures 9 and 10) as the rotated breakaway of the HHD, which is inconsistent with our interpretation of the extensional allochthons. If the HHD had a breakaway at location *d* (Figures 9 and 10), extensional allochthons would rest exactly on that breakaway segment, which is quite unlikely. We therefore argue that the breakaway is likely to be located somewhere more toward the continent.

## 5. Discussion and Conclusions

[35] We have reviewed the kinematic framework and investigated the seismic expression of top-basement detachment faults at a crustal level in magma-poor margins on the basis of outcrop evidence from the ancient Tethyan margins.

We have applied these insights to reinterpret a crucial segment of Lusigal 12 imaging the most distal continental margin in the Iberia Abyssal Plain.

### 5.1. Crustal Top-Basement Detachments and Their Seismic Expression

[36] Given the analogies of the top-basement detachments in the Tethyan and Iberian margins, such detachment faults can be considered as integral features of magma-poor margins. Given the amount of extension accommodated by these detachments, they are of great tectonic significance, but difficult to identify on seismic profiles, since they cannot readily be discerned from the undisturbed top of the acoustic basement. Our results indicate that the seismic expression of locally occurring extensional allochthons is quite characteristic and hence a suitable indicator for the detection and interpretation of top-basement detachment faults in seismic data. Extensional allochthons, which cap segments of the exposed Err detachment, are generally too small to be imaged deterministically. They do, however, give rise to pronounced individual diffractions in synthetic CMP-stacked data, which do not occur in the neighboring, exhumed segments of the Err detachment. Time-migrated synthetic seismic profiles show the capped segments as a fragmented top-basement reflection of variable strength, which alternates with a continuous, constant amplitude top-basement reflection from the top of the uncapped, exhumed detachment. A careful review of the Lusigal 12

seismic profile across the Iberia Abyssal Plain reveals very similar seismic patterns continentward of Hobby High (ODP Sites 900, 1067, and 1068). Using these diagnostic features as a guide for a reassessment of the corresponding Lusigal 12 segment leads to the interpretation of the HHD as a top-basement detachment structure.

## 5.2. Implications for the Interpretation of the Lusigal 12 Profile

[37] The identification of extensional allochthons and the interpretation of post-detachment high-angle normal faults have major implications for our geological understanding of the distal margin in the Iberia Abyssal Plain.

[38] 1. The existence of extensional allochthons 8 km to the east of Hobby High confirms the overall interpretation of HHD as a top-basement detachment fault, but contradicts the interpretation of a breakaway occurring at this location [Manatschal *et al.*, 2001]. A breakaway of HHD must therefore be located closer to the continent, which implies an even larger offset along this fault and hence a thicker pre-HHD crust than proposed by Manatschal *et al.* [2001].

[39] 2. The onlap of the oldest sediments onto the post-detachment high-angle faults and the sealing of these faults by younger sedimentary sequences (Figure 10) implies that

the sediments are postrift in age. This supports the idea proposed by Wilson *et al.* [2001] that “true” synrift sediments are rare in the distal margin, which may be explained either by very low sedimentation rates or by a very fast extension rates accommodated by the downward-concave detachment faults.

[40] 3. The postdetachment high-angle normal faults indicate an extensional process in the margin after breakup. Given the sealing of these faults by the oldest sediments, such an extension can not be much younger than breakup. On the basis of the presented data, it remains unclear whether this behavior is a local phenomenon or whether it is of a systematic and general nature. That is, either the high-angle faults are of local origin resulting from an upwarping of Hobby High, or they reflect a general postrift extensional phase within the entire distal margin.

[41] **Acknowledgments.** Our work was financed by the Swiss Federal Institute of Technology (ETH Project 0-20511-98) and was associated with the Swiss National Science Foundation project “Comparative anatomy of passive continental margins: Iberia and Eastern Alps” (20-055284-98). We thank F. Anselmetti for stimulating discussions and critically reading the manuscript. We used Seismic Unix [Cohen and Stockwell, 2000] for seismic modeling and processing purposes. EOST contribution 2002.502-UMR7517.

## References

- Alford, R. M., K. R. Kelly, and D. M. Boore, Accuracy of finite-difference modeling of the acoustic wave equation, *Geophysics*, 39, 834–842, 1974.
- Beslier, M.-O., Seismic line LG12 in the Iberia Abyssal Plain, *Proc. Ocean Drill. Program Sci. Results*, 149, 737–740, 1996.
- Buck, W. R., Flexural rotation of normal faults, *Tectonics*, 7, 959–973, 1988.
- Cohen, J. K., and J. W. Stockwell, CWPSU: Seismic Unix Release 34: A free package for seismic research and processing, Cent. for Wave Phenomena, Colo. Sch. of Mines, Golden, Colo., 2000.
- Desmurs, L., G. Manatschal, and D. Bernoulli, The Steinmann trinity revisited: Mantle exhumation and magmatism along an ocean-continent transition: The Platta nappe, eastern Switzerland, in *Non-Volcanic Rifting of Continental Margins: A Comparison of Evidence from Land and Sea*, edited by R. C. L. Wilson *et al.*, *Geol. Soc. Spec. Publ.*, 187, 235–266, 2001.
- Dolan, S. S., C. J. Bean, and B. Rioulet, The broad-band fractal nature of heterogeneity in the upper crust from petrophysical logs, *Geophys. J. Int.*, 132, 489–507, 1998.
- Ferreiro Mählmann, R., Correlation of very low grade data to calibrate a thermal maturity model in a nappe tectonic setting, a case study from the Alps, *Tectonophysics*, 334, 1–33, 2001.
- Florineth, D., and N. Froitzheim, Transition from continental to oceanic basement in the Tasna nappe (Engadine window, Graubünden, Switzerland): Evidence for Early Cretaceous opening of the Valais ocean, *Schweiz. Mineral. Petrogr. Mitt.*, 74, 437–448, 1994.
- Frankel, A., and R. W. Clayton, Finite difference simulations of seismic scattering: Implications for the propagation of short-period seismic waves in the crust and models of crustal heterogeneity, *J. Geophys. Res.*, 91, 6465–6489, 1986.
- Froitzheim, N., and G. P. Eberli, Extensional detachment faulting in the evolution of a Tethys passive continental margin, Eastern Alps, Switzerland, *Geol. Soc. Am. Bull.*, 102, 1297–1308, 1990.
- Froitzheim, N., and G. Manatschal, Kinematics of Jurassic rifting, mantle exhumation, and passive-margin formation in the Austroalpine and Penninic nappes (eastern Switzerland), *Geol. Soc. Am. Bull.*, 108, 1120–1133, 1996.
- Froitzheim, N., and D. Rubatto, Continental breakup by detachment faulting: Field evidence and geochronological constraints (Tasna nappe, Switzerland), *Terra Nova*, 10, 171–176, 1998.
- Froitzheim, N., S. M. Schmid, and P. Conti, Repeated change from crustal shortening to orogen-parallel extension in the Austroalpine units of Graubünden, *Eclogae Geol. Helv.*, 87, 559–612, 1994.
- Furrer, H., B. Aemissegger, G. P. Eberli, U. Eichenberger, S. Frank, H. Näf, and R. Trümpy, Field workshop on Triassic and Jurassic sediments in the Eastern Alps of Switzerland, *Mitt. Geol. Inst. Eidg. Tech. Hochschule. Univ. Zürich, Rep. NF 248*, 1985.
- Goff, J. A., and J. W. Jennings, Improvement of Fourier-based unconditional and conditional simulations for band limited fractal (von Kármán) statistical models, *Math. Geol.*, 31, 627–649, 1999.
- Goff, J. A., and T. H. Jordan, Stochastic modeling of seafloor morphology: Inversion of sea beam data for second-order statistics, *J. Geophys. Res.*, 93, 13,589–13,608, 1988.
- Hölker, A. B., K. Holliger, G. Manatschal, and F. Anselmetti, Seismic reflectivity of detachment faults of the Iberian and Tethyan distal continental margins based on geological and petrophysical data, *Tectonophysics*, 350, 127–156, 2002.
- Holliger, K., Upper-crustal seismic velocity heterogeneity as derived from a variety of p-wave sonic logs, *Geophys. J. Int.*, 125, 813–829, 1996.
- Holliger, K., Seismic scattering in the upper crystalline crust based on evidence from sonic logs, *Geophys. J. Int.*, 128, 65–72, 1997.
- Holliger, K., and A. Levander, Structure and seismic response of extended continental crust: Stochastic analysis of the Strona-Ceneri and Ivrea zones, Italy, *Geology*, 22, 79–82, 1994.
- Holliger, K., A. R. Levander, and J. A. Goff, Stochastic modeling of the reflective lower crust: Petrophysical and geological evidence from the Ivera Zone (Northern Italy), *J. Geophys. Res.*, 98, 11,967–11,980, 1993.
- Kelly, K. R., R. W. Ward, S. Treitel, and R. M. Alford, Synthetic seismograms: A finite-difference approach, *Geophysics*, 41, 2–27, 1976.
- Lavier, L. L., W. R. Buck, and A. N. B. Poliakov, Self-consistent rolling-hinge model for the evolution of large-offset low-angle normal faults, *Geology*, 27, 1127–1130, 1999.
- Lister, G. S., and G. A. Davis, The origin of metamorphic core complexes and detachment faults formed during Tertiary continental extension in the northern Colorado River region, U. S. A., *J. Struct. Geol.*, 11, 65–94, 1989.
- Manatschal, G., Fluid- and reaction-assisted low-angle normal faulting: Evidence from rift-related brittle fault rocks in the Alps (Err Nappe, eastern Switzerland), *J. Struct. Geol.*, 21, 777–793, 1999.
- Manatschal, G., and D. Bernoulli, Architecture and tectonic evolution of an oceanic margin: Present-day Galicia and ancient Adria, *Tectonics*, 18, 1099–1119, 1999.
- Manatschal, G., and P. Nievergelt, A continent-ocean transition recorded in the Err and Platta nappes (Eastern Switzerland), *Eclogae Geol. Helv.*, 90, 3–27, 1997.
- Manatschal, G., N. Froitzheim, M. J. Rubenach, and B. D. Turin, The role of detachment faulting in the formation of an ocean-continent transition: Insights from the Iberia Abyssal Plain, in *Non-Volcanic Rifting of Continental Margins: A Comparison of Evidence From Land and Sea*, edited by R. C. L. Wilson *et al.*, *Geol. Soc. Spec. Publ.*, 187, 405–428, 2001.
- Martini, F., C. J. Bean, S. Dolan, and D. Marsan, Seismic image quality beneath strongly scattering structures and implications for lower crustal imaging:

- Numerical simulations, *Geophys. J. Int.*, *145*, 423–435, 2001.
- Taylor, B., et al., *Proceedings of the Ocean Drilling Program, Initial Reports*, vol. 180 [CD-ROM], Ocean Drill. Program, College Station, Tex., 1999.
- von Kármán, T., Progress in the statistical theory of turbulence, *J. Mar. Res.*, *7*, 252–264, 1948.
- Whitmarsh, R. B., and P. J. Wallace, The rift-to-drift development of the West Iberia nonvolcanic continental margin: A summary and review of the contribution of Ocean Drilling Program Leg 173, *Proc. Ocean Drill. Program Sci. Results*, *173*, 1–36, 2001.
- Whitmarsh, R. B., et al., *Proceedings of the Ocean Drilling Program, Initial Reports*, vol. 173, Ocean Drill. Program, College Station, Tex., 1998.
- Whitmarsh, R. B., S. M. Dean, T. A. Minshull, and M. Tompkins, Tectonic implications of exposure of lower continental crust beneath the Iberia Abyssal Plain, Northeast Atlantic Ocean: Geophysical evidence, *Tectonics*, *19*, 919–942, 2000.
- Whitmarsh, R. B., G. Manatschal, and T. A. Minshull, Evolution of magma-poor continental margins from final rifting to seafloor spreading, *Nature*, *413*, 150–154, 2001.
- Wilson, R. C. L., G. Manatschal, and S. Wise, Rifting along non-volcanic passive margins: Stratigraphic and seismic evidence from the Mesozoic successions of the Alps and western Iberia, in *Non-Volcanic Rifting of Continental Margins: A Comparison of Evidence from Land and Sea*, edited by R. C. L. Wilson et al., *Geol. Soc. Spec. Publ.*, *187*, 429–452, 2001.
- 
- D. Bernoulli, Department of Earth Sciences, University of Basel, Bernoullistr. 32, CH-4056 Basel, Switzerland.
- A. B. Hölker, Proseis AG, Siewerdstr. 7, CH-8050, Zurich, Switzerland. (hoelker@proseis.com)
- K. Holliger, Institute of Geophysics, Department of Earth Sciences, Swiss Federal Institute of Technology, ETH-Hönggerberg, CH-8093 Zurich, Switzerland.
- G. Manatschal, CGS-EOST, CNRS-Université Louis Pasteur, 1 rue Blessig, F-67084 Strasbourg, France.